7(2010) 369 – 389

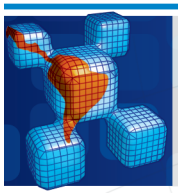

Latin American Journal of Solids and Structures
www.lajss.org

Behavior analysis of bar gaps in welded YT-joints for rolled-steel circular hollow sections

Abstract

We present a parametric analysis of gap variation between the lap brace and through brace of YT welded joints for rolled-steel circular hollow sections on plane steel structures. Our aim is to investigate the collapse behavior of YT-joints under lap brace axial compression. In particular, we focus on e/d_0 ratios above 0.25 so bending moments can be taken into account during the design. We find that joint failure is primarily due to chord wall plastification (Mode A) and cross-sectional chord buckling (Mode F) in the region underneath the lap brace. Our joint design followed the Limit States Method, and our results were based on a comparative analysis of three different methods: an analytical solution derived from a set of international technical norms, an experimental analysis, and numerical modeling using Ansys as calibrated by our experimental results.

Keywords

Circular hollow sections, joint, bar gap, finite-element analysis, parametric study.

R.F. Vieira[a,*], **J.A.V. Requena**[a], **A. M. S. Freitas**[b] **and V. F. Arcaro**[a]

[a] State University of Campinas, Campinas, SP – Brazil
[b] Federal University of Ouro Preto, Ouro Preto, MG – Brazil

Received 12 Mar 2010;
In revised form 8 Dez 2010

* Author email: rosilenefv@gmail.com

1 INTRODUCTION

The extensive use of steel frame structures is primarily due to the economic advantages of manufacturing steel frames. In this work, we study the strength of connection joints for tubular steel frames as a function of gap length between the lap and through braces of YT-joints. This work extends earlier studies of tubular joints that focused on experimental tests [5], theoretical analyses using the Finite Element Method [2–4], and analytical work aimed at developing mathematical expressions of the joint strength [6].

2 CALCULATION OF CONNECTION RESISTANCE

The YT joint prototype design uses the methodology presented by Wardenier et al. [10] and Packer and Henderson [7].

The Fig. 1 shows forces general scheme using as a limit the maximum capacity of the vertical brace member of the YT joint and the bending moment due the eccentricity was not considered [9].

NOMENCLATURE

A_i	cross sectional area of member i ($i = 0, 1, 2, 3$);
E	modulus of elasticity;
E_t	modulus of elasticity tangent;
M_0	bending moment in the chord member;
N_i	axial force applied to member i ($i = 0, 1, 2, 3$);
N_i^*	joint design resistance expressed in terms of axial load in member i;
N_{0P}	pre-stressing axial force on the chord;
W_0	elastic section modulus of member i ($i = 0, 1, 2, 3$);
d_i	external diameter of circular hollow section for member i ($i = 0, 1, 2, 3$);
e	nodding eccentricity for a connection;
f_y	yield stress;
f_{yi}	yield stress of member i ($i = 0, 1, 2, 3$);
f_{0P}	pre-stress in chord;
$f(n')$	function which incorporates the chord pre-stress in the joint resistance equation;
g	gap between the bracings members of a K, N or KT joint, at the face of the chord;
g'	gap divided by chord wall thickness;
n'	$\frac{f_{0P}}{f_{y0}} = \frac{N_{0P}}{A_0 \cdot f_{y0}} + \frac{M_0}{W_0 \cdot f_{y0}}$
t_i	thickness of hollow section member i ($i = 0, 1, 2, 3$);
β	diameter ratio between bracing on chord;
	$\beta = \frac{d_1}{d_0}, \frac{d_1}{b_0}, \frac{b_i}{b_0}$ T, Y and X
	$\beta = \frac{d_1+d_2}{2 \cdot d_0}, \frac{d_1+d_2}{2 \cdot b_0}, \frac{b_1+b_2+h_1+h_2}{4 \cdot b_0}$ K and N
γ	ratio of the chord's half diameter to its thickness;
ν	Poisson's ratio
θ	included angle between bracing member i ($i = 0, 1, 2, 3$) and the chord;
ϵ	maximum specific proportionality strain;
f	stress;
f_{lp}	maximum proportionality stress;
f_r	maximum resistance stress;
f_1	principal stress 1;
f_2	principal stress 2;

Table 1 shows the geometric characteristics of the VMB 250 circular hollow sections used in the YT joint. The nominal physical proprieties yield stress (f_y) are equal 250 MPa.

2.1 Validity limits

The YT joint meets all geometrical requirements described in the aforementioned references.

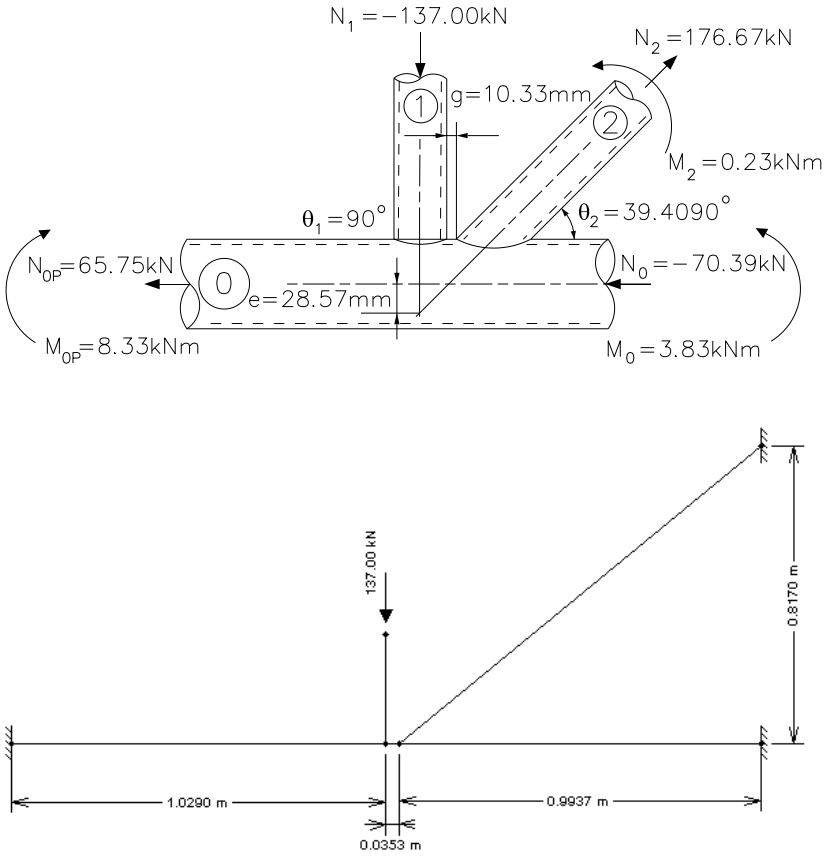

Figure 1 Forces general scheme of YT joint.

Table 1 Physical and geometrical characteristics.

Member	**Hollow Section**	**Thickness**	**Area**	**Elastic resistant modulus**	**Load**
	mm	**mm**	**mm^2**	**mm^3**	**kN**
Chord	ϕ114.3	#6.02	2047.83	52677.51	N_0 = - 70.39 N_{0P} = 65.75
Lap brace	ϕ73.0	#5.16	1099.73	17433.30	N_1= -137.00
Through brace	ϕ73.0	#5.16	1099.73	17433.30	N_2=176.67

2.2 Calculations

A) YT joint parameters

The YT joint parameters are given by Eq. (1) through Eq. (5):

$$\beta = \frac{d_1 + d_2}{2 \cdot d_0}; \tag{1}$$

$$g' = \frac{g}{t_0}; \tag{2}$$

The stress on the chord, f_{0P}, depends most critically on the compressing stress.

$$n' = \frac{f_{0P}}{f_{y0}} = \frac{N_{0P}}{A_0 \cdot f_{y0}} + \frac{M_0}{W_0 \cdot f_{y0}}; \tag{3}$$

$$f\ (n') = 1.0 + 0.3 \cdot n' \ - \ 0.3 \cdot n'^2 \ \leq \ 1\,; \tag{4}$$

$$f\ (\gamma, g') = \gamma^{0.2} \cdot \left(1 + \frac{0.024 \cdot \gamma^{1.2}}{1 + \exp^{(0.5 \cdot g' \ - \ 1.33)}}\right); \tag{5}$$

B) Plastic failure of the chord face (Mode A)

Vertical lap brace:

$$N_1^* = \frac{f_{y0} \cdot t_0^2}{sen\theta_1} \left(1.8 + 10.2 \cdot \frac{d_1}{d_0}\right) \cdot f\ (\gamma, g')\ \cdot\ f\ (n')\ ; \tag{6}$$

Diagonal through brace:

$$N_2^* = N_1^*\ \cdot \left(\frac{sen\theta_1}{sen\theta_2}\right); \tag{7}$$

C) Punching shear failure of the chord face (Mode B)

Vertical lap brace and diagonal through brace are both given by Eq. (8):

$$N_i^* = \frac{f_{y0} \cdot t_0 \cdot \pi \cdot d_i}{\sqrt{3}}\ \cdot \left(\frac{1 + sen\theta_i}{2 \cdot sen^2\theta_i}\right); \tag{8}$$

D) YT Joint Resistance

The joint resistance is the lowest value obtained in items (B) and (C) above.

Vertical lap brace:

$$\frac{N_1}{N_1^*} < 1; \tag{9}$$

Diagonal through brace:

$$\frac{N_2}{N_2^*} < 1; \tag{10}$$

Table 2 presents the results of the calculation.

Table 2 Results of the calculation procedure.

Joint parameters	**Acronym**	**Calculation**
Relation between diameters	β	0.64
Relation between diameter and thickness	γ	9.49
$n' = \text{stress}/f_y$ (compression)	n'	-0.14
Function of prestress on chord	$f(n')$	0.95
Resistance plastic failure of the chord face (Mode A)	$N_1^*(Pl)$	137.40 kN
Resistance punching shear failure of the chord face (Mode B)	$N_1^*(Pu)$	199.27 kN
Lap brace use	N_1/N_1^*	1.0
Resistance plastic failure of the chord face (Mode A)	$N_2^*(Pl)$	216.42 kN
Resistance punching shear failure of the chord face (Mode B)	$N_2^*(Pu)$	404.16 kN
Through brace use	N_2/N_2^*	0.82

3 EXPERIMENTAL PROGRAM

To study the joint, four prototypes constructed from seamless rolled tubes were manufactured by V&M do Brasil. They were called pre-experiment, experiments I, II and III [9].

3.1 YT joint prototypes

The dimensions of the prototypes are shown in Fig. 2. The prototypes are fixed by four screws at each end. They were loaded axially at the top of the lap brace.

3.2 Instrumentation for tests

In EXPERIMENTS I, II and III, sixteen 5mm electrical resistance KFG-5-120-C1-11 extensometers were used. Their positions are marked EER1 to EER16 in Fig. 3.

The EERs were placed on the prototype to measure longitudinal strain, drawing on the work of Fung et al [5]. In EXPERIMENT III, 2 rosette gauges and 2 individual extensometers were added (for a total of 24 EERs). Rosette 1 was composed of EER20, EER21 and EER22; rosette 2 was composed of EER17, EER18 and EER19. EER23 and EER24 were placed at the bases of the lap brace and through brace respectively.

In EXPERIMENTS I, II and III, 19 manual reading displacement transducers (TD1 to TD19) and two digital reading displacement transducers (TD20 and TD21) were placed on the prototype as shown in Fig. 4.

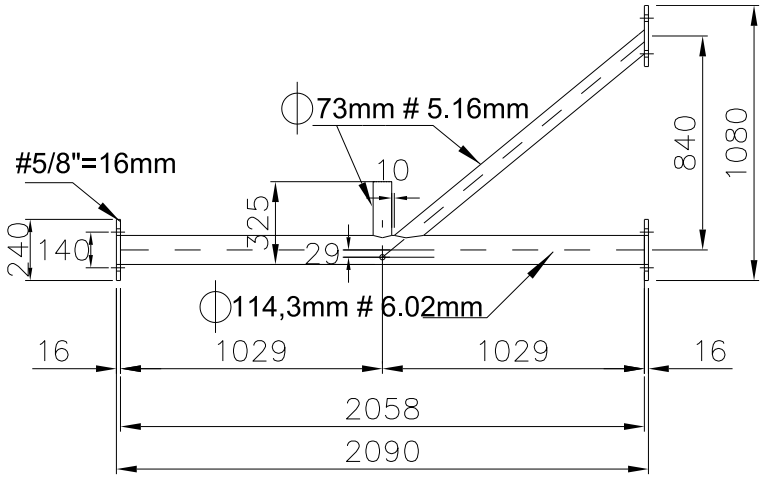

Figure 2 YT joint prototype (mm).

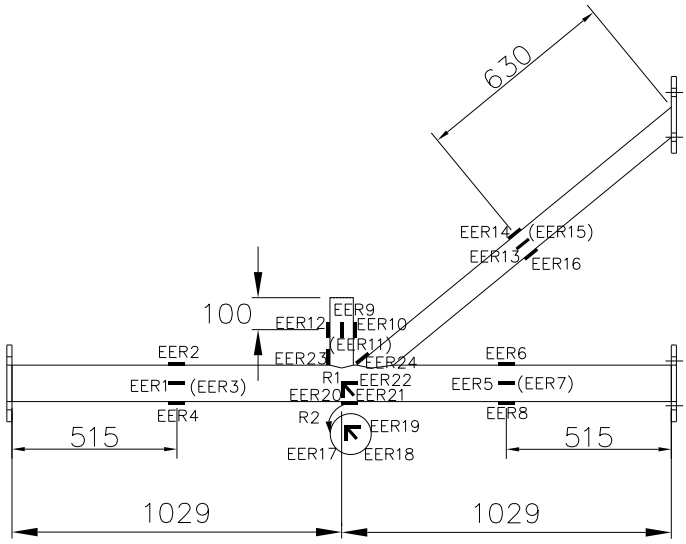

Figure 3 Positioning of the extensometers on the YT joint prototype.

3.3 Experimental results

The testing methodology used was defined in three stages, as shown below:

Stage I. Before starting the test, the prototype was subjected to a cycle of 10 loading of approximately 20% of the estimated collapse loading for the connection, to minimize friction and check the torque of the screws. Based on pre-test the loading was estimated at 50kN. This level of loading is within the elastic limit of the material. The force was applied in small increments and then it was done downloading.

Stage II. During the test the speed of the actuator load was kept as slow and steady as possible

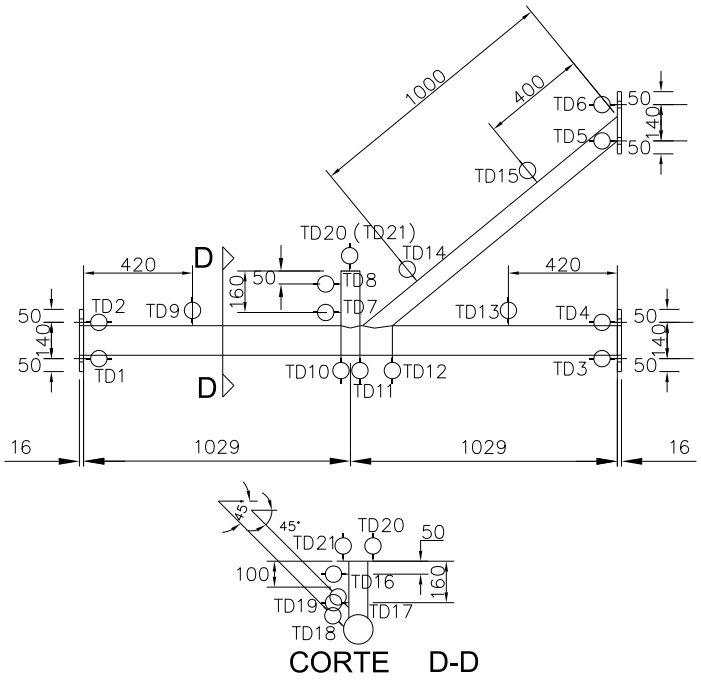

Figure 4 Positioning of the DTs on the YT joint prototype.

for both the case of loading and for unloading. The step load was previously set depending on the stage supposed to loading. At each step of loading, when the pre established loading was reached, expected time to stabilize the transducers and then did the reading.

Stage III. The prototype was loaded to the ultimate state, where the prototype did not offer more resistance, even after he reached the break. Then the prototype was unloaded.

Fig. 5 shows the overall strain of the prototype in EXPERIMENT III, characterized by the development of failure Mode A.

The results presented by extensometers in each EXPERIMENTS I, II and III are similar, are representing the state of tension expected for each region and thus show that the tests were equivalent.

The results of the last loading for each of the tests are shown in Table 3.

Table 3 Last loading to EXPERIMENTS I, II and III.

EXPERIMENTS	**Last loading (kN)**
EXPERIMENT I	240.0
EXPERIMENT II	358.6
EXPERIMENT III	316.4

Figure 5 Overall strain of the prototype for EXPERIMENT III.

Two failure modes were observed: plastic failure of the chord face (Mode A) and local buckling of the chord walls (Mode F).

4 ANALYSIS OF FINITE ELEMENTS

Two numerical models were created in Ansys [1], one using a bilinear stress-strain diagram (BISO – Bilinear Isotropic Hardening) and the other a multilinear (piecewise linear) diagram (MISO – Multilinear Isotropic Hardening). Their results were compared to the experimental tests [9].

Both physical and geometrical non-linearity were considered in the analysis. To implement physical non-linearity, we used the stress-strain diagrams obtained through test-body traction. Test bodies cp1a, cp1b for hollow section of diameter 73mm and cp2a e cp2b for hollow section of diameter 114.3mm [9].

The contour conditions were simulated in Ansys through displacement restrictions. Force was applied in an increasing way, that is, at unit load pitches.

Fig. 6 and Fig. 7 show the stress-strain diagrams of test bodies selected for the numerical analysis. The multilinear model is represented by 26 points (crossed circles), and the bilinear model by two straight lines (triangles).

Table 4 shows data used to represent the material properties of test bodies cp1b and cp2b in the numerical model. Note that the bilinear stress-strain diagram always runs from the origin to the first stress peak (f), then from this point to the maximum stress (f_r) of the material.

The 26 points to represent the multilinear stress-strain diagram is shown by Table 5.

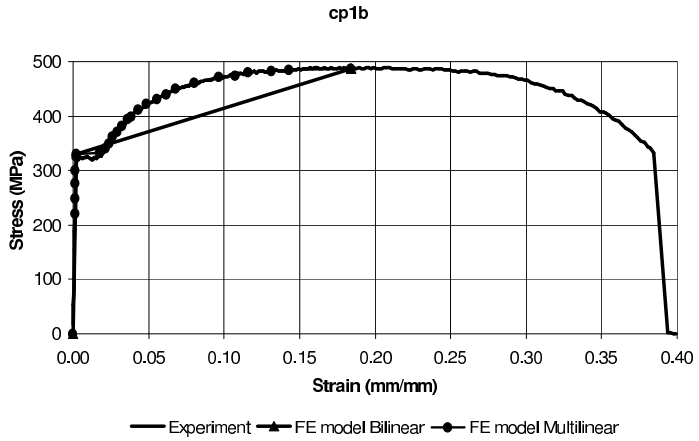

Figure 6 Experimental, bilinear and multilinear stress-strain diagrams used for test body cp1b, from the through brace and lap brace (ϕ73mm).

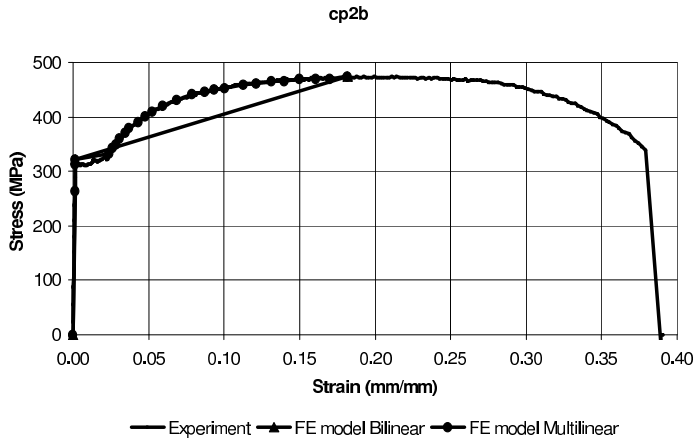

Figure 7 Experimental, bilinear and multilinear stress-strain diagrams used for test body cp2b, from the chord (ϕ114.3mm).

Table 4 Data used to represent the bilinear stress-strain diagram with the Ansys software (BISO).

Test Body	f_y	f	f_r	E	E_t
	(MPa)	(MPa)	(MPa)	(MPa)	(MPa)
cp1b(ϕ73mm)	326.0	331.1	486.9	189114.6	856.5
cp2b(ϕ114.3mm)	322.6	322.6	473.6	227390.8	840.6

Table 5 Data used to represent the multilinear stress-strain diagram with the Ansys software (MISO).

Points	cp1b(ϕ73mm)			cp2b(ϕ114,3mm)		
	ε (Dimensionless)	f (GPa)	E (GPa)	ε (Dimensionless)	f (GPa)	E (GPa)
0	0	0	0	0	0	0
1	0.001165	0.22031	189.1146	0.001165	0.2649	227.3908
2	0.0013373	0.24958	186.6298	0.0014234	0.31285	219.7906
3	0.0015613	0.27689	177.3458	0.0017508	0.32257	184.2415
4	0.0017853	0.29975	167.899	0.023651	0.33273	14.06833
5	0.001992	0.32604	163.6747	0.026081	0.34245	13.13025
6	0.0022849	0.3311	144.9079	0.028562	0.3501	12.25754
7	0.017672	0.3324	18.80942	0.031181	0.3607	11.56794
8	0.021394	0.34219	15.99467	0.034834	0.37027	10.62956
9	0.023668	0.35058	14.8124	0.037418	0.38073	10.17505
10	0.026442	0.36218	13.69715	0.043173	0.39133	9.06423
11	0.029286	0.3713	12.67841	0.047722	0.40085	8.39969
12	0.032646	0.38115	11.67524	0.052478	0.41042	7.820801
13	0.036229	0.39585	10.92633	0.059905	0.42068	7.022452
14	0.038728	0.40007	10.33025	0.068554	0.43103	6.287452
15	0.043656	0.41183	9.433526	0.0786	0.44115	5.612595
16	0.048567	0.42287	8.706941	0.0874737	0.44546	5.092552
17	0.055838	0.43131	7.72431	0.093987	0.45077	4.796089
18	0.061989	0.44038	7.104164	0.1006035	0.45302	4.50305
19	0.068227	0.4504	6.601492	0.11285	0.46019	4.077891
20	0.080736	0.46188	5.720868	0.12118	0.46171	3.810117
21	0.096589	0.47179	4.884511	0.13124	0.465	3.543127
22	0.1074614	0.47472	4.417572	0.14001	0.46647	3.331691
23	0.1159	0.48035	4.144521	0.15042	0.46932	3.120064
24	0.1316533	0.48221	3.662694	0.1611	0.4701	2.918063
25	0.14347	0.48564	3.384959	0.17035	0.47025	2.760493
26	0.18417	0.48688	2.643644	0.18148	0.47364	2.609874

The Poisson's ratio was obtained by compression test tube used. The value obtained was $\nu = 0.3$.

The SHELL element was considered most appropriate to represent hollow structures. Specifically, the SHELL181 element was used to generate a mesh for the hollow sections. The SHELL63 element was used for fixation plates. Table 6 shows their characteristics.

Table 6 Characteristics of elements.

Elements	**Nr of nodes per element**	**Degrees of freedom**	**Special features**		
SHELL 63	4	6	Elastic	Large deflection	Little strain
SHELL 181	4	6	Plastic	Large deflection	Large strain

5 COMPARISON BETWEEN EXPERIMENTAL TEST RESULTS AND NUMERICAL MODEL RESULTS

The experimental tests and numerical models can be compared on the basis of strains obtained by the extensometers [9].

For the rosettes, comparisons between theory and experiment can be made between the principal stresses.

Fig. 8 show the principal stresses f_1 measured at rosette 1 in EXPERIMENT III and the numerical models.

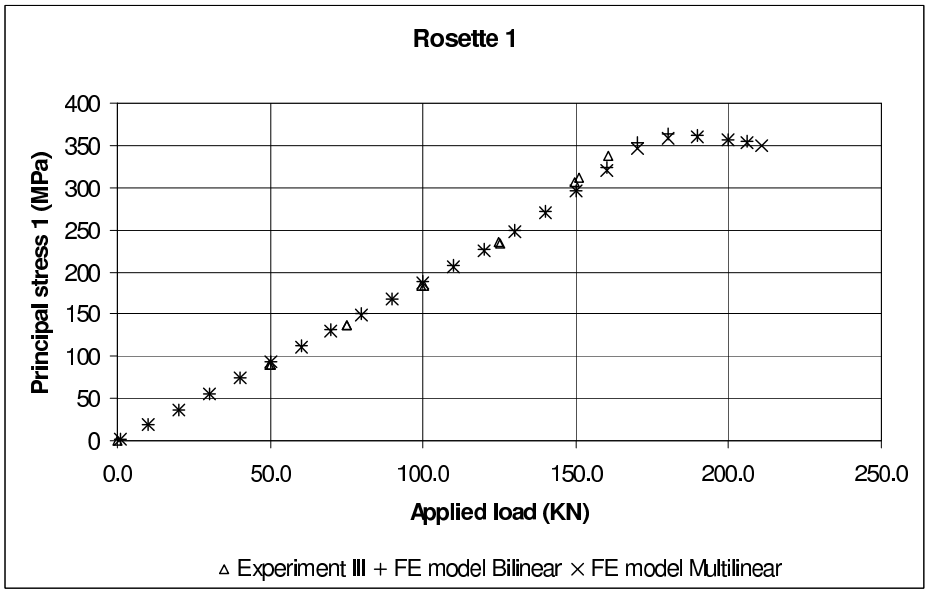

Figure 8 Principal stress f_1 measured at rosette 1 in EXPERIMENT III and the numerical models.

The principal stresses f_1 of the two numerical models were in good agreement with those obtained by rosette 1 in EXPERIMENT III.

6 METHODS USED FOR PARAMETRIC ANALYSIS

Summarizing, the overall geometry and minimum allowable gap size of the YT-joint described in this work is shown in Fig. 2. Using this schematic, we fabricated and tested four test specimens in the laboratory and generated numerical models using program Ansys. Our numerical models were calibrated using our experimental results, so as to precisely represent the predefined gap in the YT-joint [9]. These models used a SHELL181 four-node element for the tubular sections, and we took into account both material and geometric nonlinearity effects [8], the latter using a Multilinear Isotropic Hardening (MISO) material.

We performed a parametric analysis to study the effect of gap size between the lap brace and through brace on the overall strength of the YT-joint. The motivation for this study stems from the observation that the gap length can influence the resistance to chord wall plastification failure (Mode A) for YT-joints using circular hollow sections.

According to Packer and Henderson [7], the e/d_0 ratio for the joint must satisfy the limits given by Eq. (11); this represents the range over which the effects of the joint's bending moments can be disregarded, namely.

$$-0.55 \leq \left(\frac{e}{d_0}\right) \leq 0.25. \tag{11}$$

If these eccentricity boundaries are exceeded, then the generated moment has a detrimental effect on the joint strength since the moment must be distributed between the braces. If this occurs, the joint capacity must be checked for interaction between the axial force and the bending moment.

Note that for gap lengths greater than the lowest acceptable value of g=10.33 mm, we have $g \geq t_1 + t_2$ and the e/d_0 ratio exceeds the boundary condition of 0.25. Consequently, this work will focus on e/d_0 ratios between 0.25 and 0.97 when analyzing new models. Our overall focus is to study the strength YT-joints for gap lengths greater than g=10.33 mm, with emphasis on the influence of bending moments on the overall joint design.

7 GAP LENGTH MODELS

Table 7 shows the gap lengths studied here, along with their corresponding eccentricity "e" values and e/d_0 ratios.

A numeric model was generated using Ansys for each gap size; hereafter, we refer to each model using the gap size as "GAP10.33", "GAP30", "GAP50", "GAP70", "GAP90" and "GAP110".

Table 7 Gap lengths, eccentricities and e/d_0 ratios of models studied in this work.

Gap Lengths (mm)	e (mm)	e/d_0
gap=10.33 (GAP10.33)	28.57	0.25
gap =30 (GAP30)	44.73	0.39
gap=50 (GAP50)	61.17	0.54
gap=70 (GAP70)	77.60	0.68
gap=90 (GAP90)	94.03	0.82
gap=110 (GAP110)	110.47	0.97

8 RESULTS FOR THE EFFECT OF GAP LENGTH ON YT-JOINT STRENGTH

The principal stresses "f_1" for each gap size are shown in Figs. 9 through 14. For all models, the largest stresses were observed on the chord at the joint intersection.

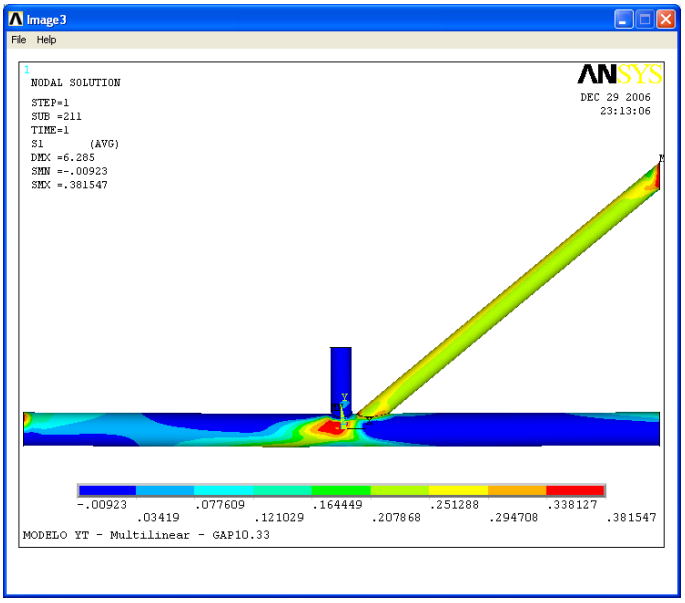

Figure 9 Principal stress "f_1" for model "GAP10.33".

Our models show that the stress distributions between the lap brace and through brace are indeed influenced by the gap size. As seen in Fig. 15, varying gap sizes from the "GAP10.33" to "GAP110" models produces approximately twice the principal stress "f_1" for the same load of 100kN.

For each model, the respective yield load was then determined based on a yield strength of $\sigma_e = 0.33$ GPa, as defined by a tensile test [8]. Table 8 shows the yield load for each of the new models. As the gap size increases, the yield load of the joint decreases, which translates into a smaller load supported on the top of the lap brace. Hence the larger the gap size, the smaller the load transfer efficiency between the braces.

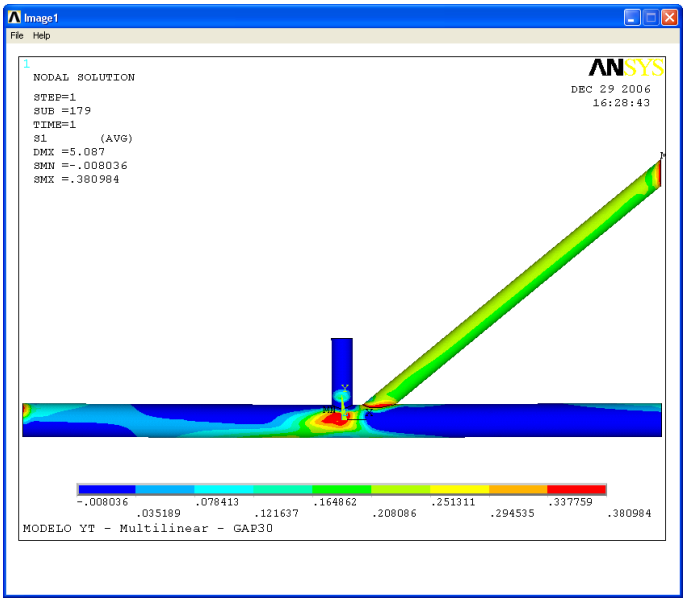

Figure 10 Principal stress "f_1" for model "GAP30".

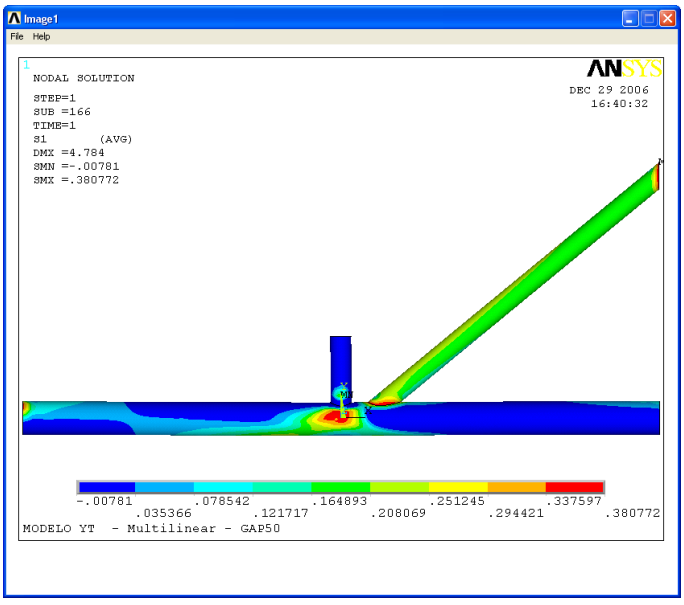

Figure 11 Principal stress "f_1" for model "GAP50".

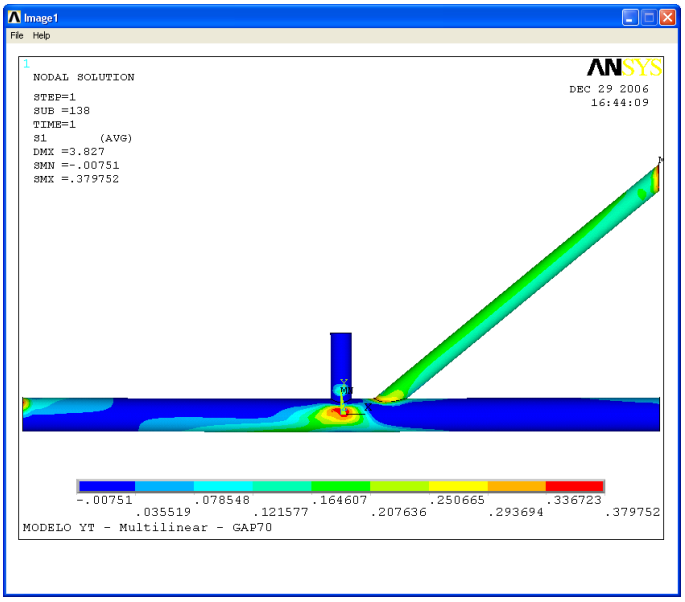

Figure 12 Principal stress "f_1" for model "GAP70".

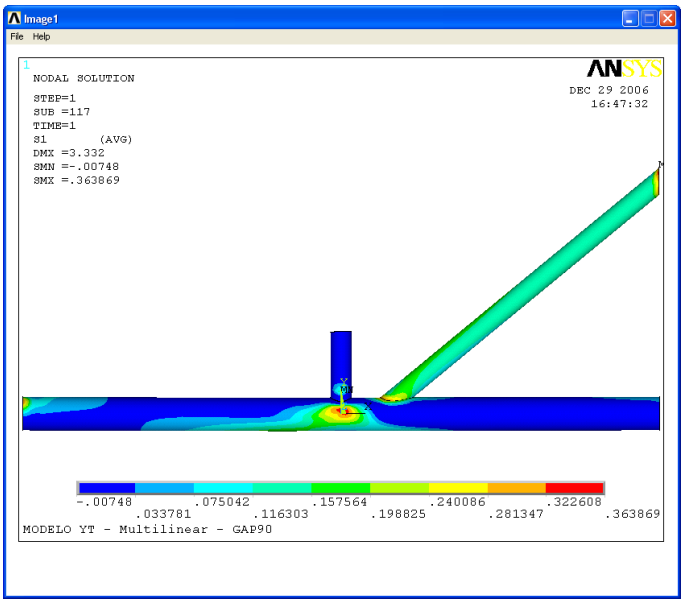

Figure 13 Principal stress "f_1" for model "GAP90".

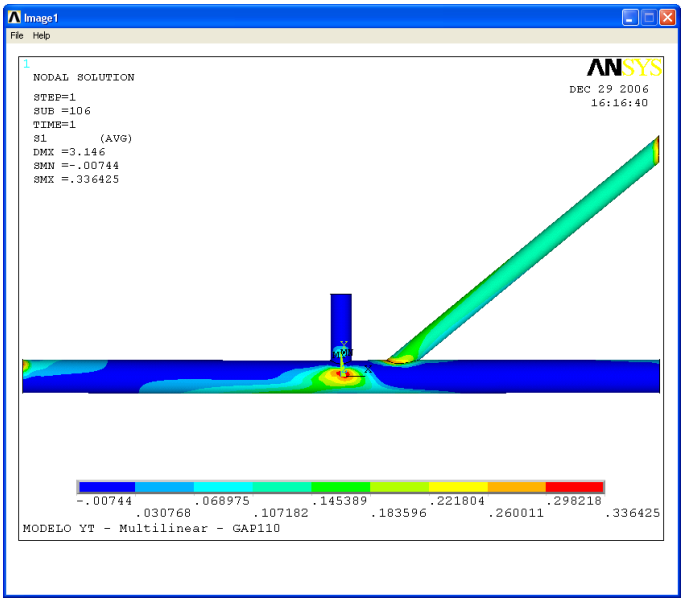

Figure 14 Principal stress "f_1" for model "GAP110".

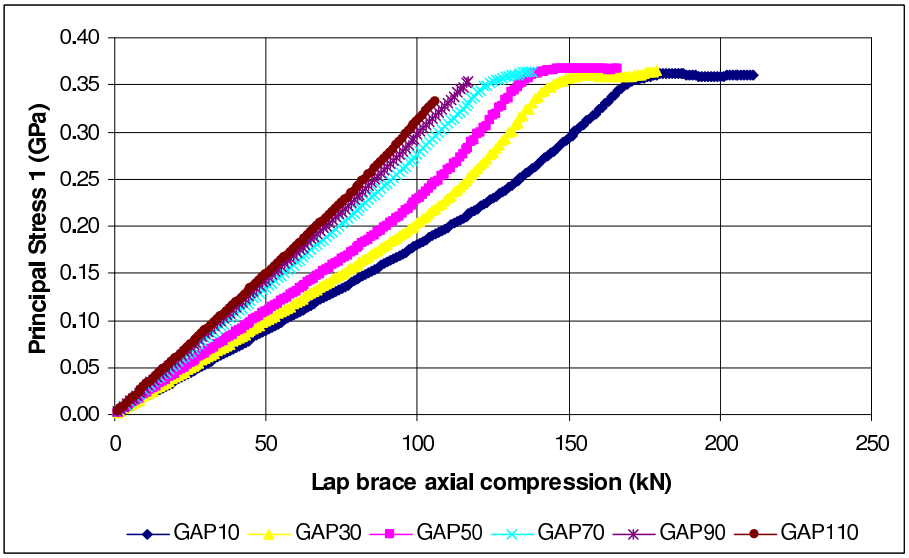

Figure 15 Principal stress "f_1" for our numeric models.

Table 8 Yield load for our numeric models.

Gap Length (mm)	Yield Load (kN)
gap=10.33 (GAP10.33)	161
gap=30 (GAP30)	131
gap=50 (GAP50)	121
gap=70 (GAP70)	115
gap=90 (GAP90)	109
gap=110 (GAP110)	104

8.1 Failure modes

The predominant failure modes for "GAP30" through "GAP110" are shown in Figs. 16 through 19, respectively. This shows that the main failure mechanisms are due to chord wall plastification (Mode A) and chord buckling (Mode F).

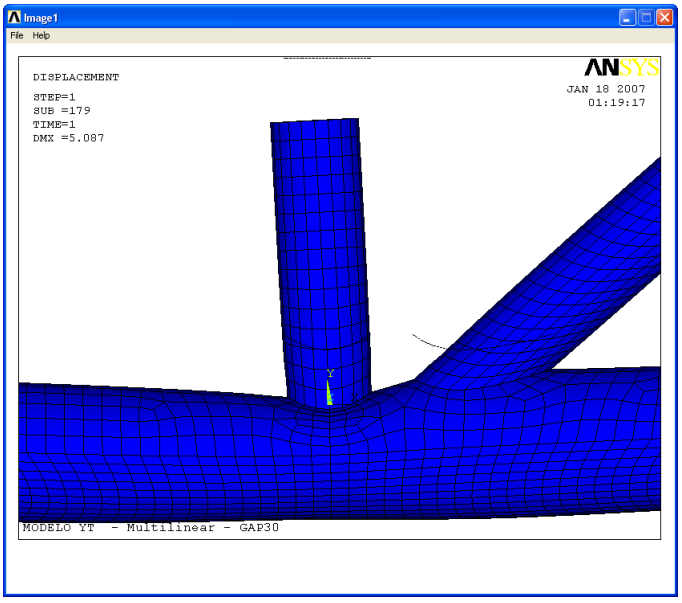

Figure 16 Plastic failure due to chord wall plastification in model "GAP30".

9 NUMERICAL ANSYS ANALYSIS OF DIMENSION LOAD VERSUS YIELD LOAD

We designed the tubular YT-joint specimen using values presented by CIDECT [10] and Packer and Henderson [7]. This gave a dimension load of 137 kN with 100% efficiency on the top of the lap brace and 82% efficiency for the through brace (Item 2). Note that we did not take bending moments into consideration during the design calculations since e/d_0=0.25.

Recall that the Mode A failure depends on the gap length. The dimension loads for each

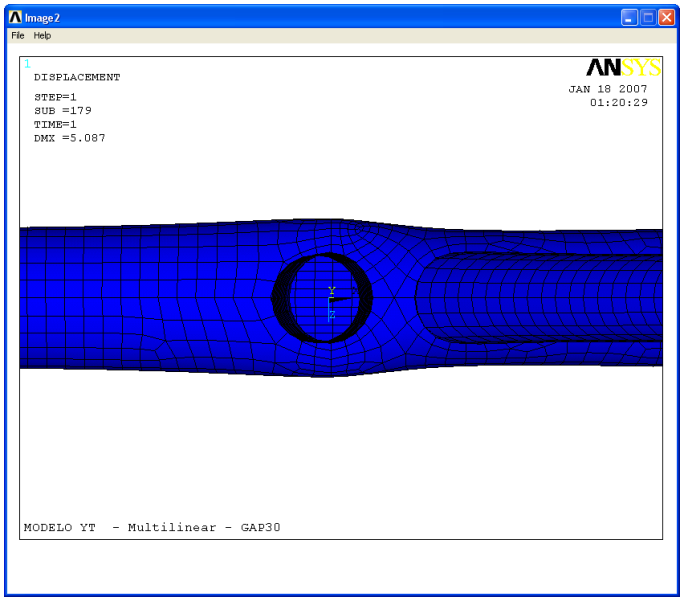

Figure 17 Chord buckling in model "GAP30".

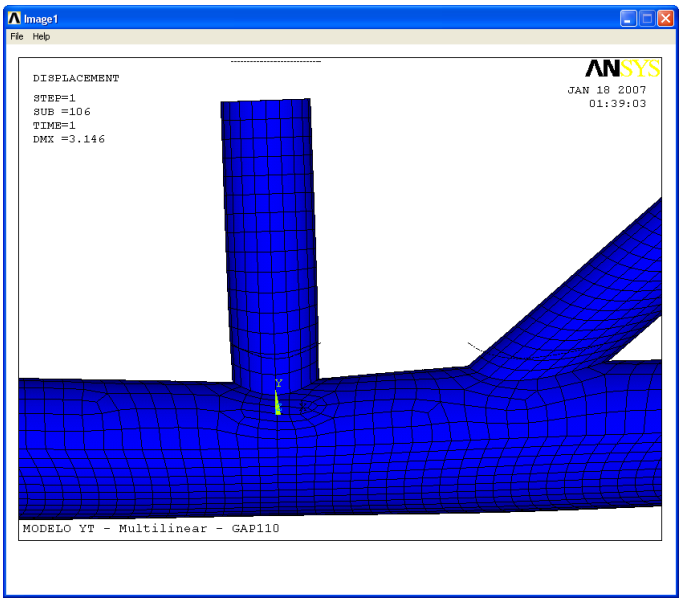

Figure 18 Plastic failure due to chord wall plastification in model "GAP110".

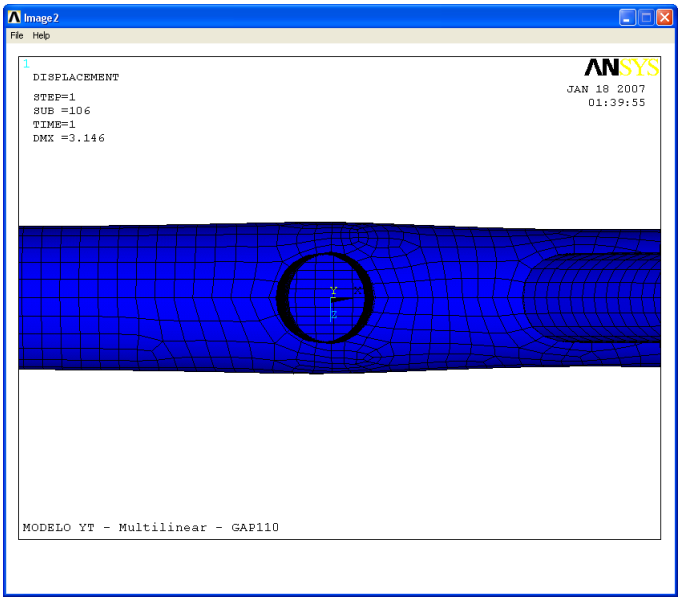

Figure 19 Chord buckling in model "GAP110".

of the new models were calculated in the same way as before, except that we took bending moments into consideration since $e/d_0 > 0.25$. We compared the results with the yield loads supplied by Ansys, and our results are presented in Fig. 20.

Table 9 shows the values of dimension load, yield load and the percent difference between them.

Table 9 Dimension load, yield load and percent difference between them.

Gap Model	**Dimension Load (kN)**	**Yield Load (kN) Ansys**	**Percent Difference**
GAP10.33	137	161	17.52%
GAP30	114	131	14.91%
GAP50	112	121	8.04%
GAP70	113	115	1.77%
GAP90	111	109	-1.80%
GAP110	108	104	-3.70%

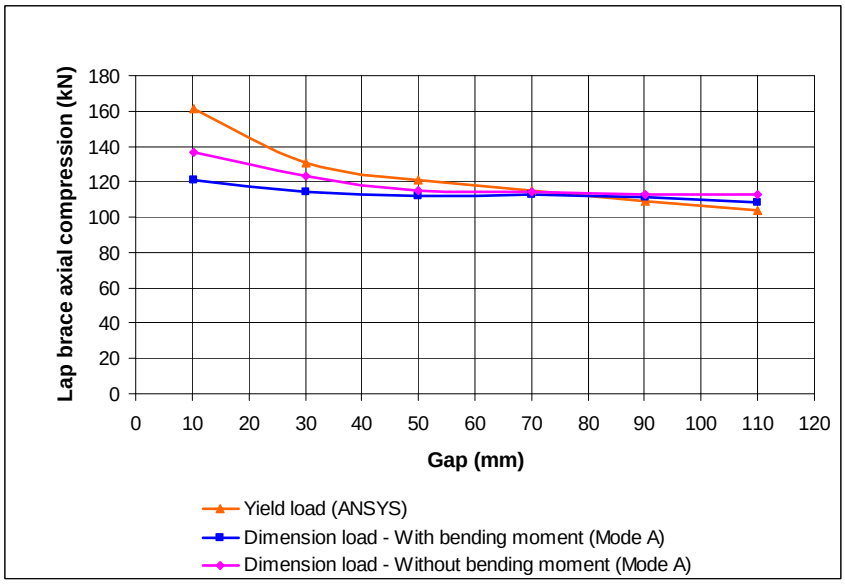

Figure 20 Dimension load and yield load.

10 CONCLUSIONS

We found that variation in gap lengths do not alter the principal failure mode for YT-joints. The principal failure modes are due to wall chord plastification (Mode A) and chord buckling (Mode F) regardless of the gap length. For gap lengths between g=10.33 mm and g=110 mm, the percent difference between the dimension load and the yield load decreases as the gap length increases. For gap values up to g=70 mm, the yield load of the numerical model is above the dimension load, implying that such designs are safe. For gap lengths greater than g=70 mm, the yield load falls short of the dimension load, implying that such designs are unsafe and the existing formulations of such joint designs should be reexamined.

Acknowledgements The authors are grateful for the support from UNICAMP, from Vallourec & Mannesmann Tubes (V&M do Brasil).

References

[1] ANSYS. Inc. *Theory reference, version 9.0.* 2004.

[2] E. M. Dexter and M. M. K. Lee. Static strength of axially loaded tubular K-joint. I: Behaviour. *Journal of Structural Engineering*, 125(2):194–201, 1999.

[3] E. M. Dexter and M. M. K. Lee. Static strength of axially loaded tubular K-joint. II: Ultimate capacity. *Journal of Structural Engineering*, 125(2):202–210, 1999.

[4] T. C. Fung, C. K. Soh, and W. M. Gho. Ultimate capacity of completely overlapped tubular joints – II. Behavioural study. *Journal of Constructional Steel Research*, 57(8):881–906, 2001.

[5] T. C. Fung, C. K. Soh, W. M. Gho, and F. Qin. Ultimate capacity of completely overlapped tubular joints – I. An experimental investigation. *Journal of Constructional Steel Research*, 57(8):855–880, 2001.

[6] Y. Kurobane, Y. Makino, and K. Ochi. Ultimate resistance of unstiffened tubular joints. *Journal of Structural Engineering*, 110(2):385–400, 1984.

[7] J. A. Packer and J. E. Henderson. *Hollow structural section connections and trusses: a design guide*. Canadian Institute of Steel Construction, Ontario, 2nd edition, 1997.

[8] R. F. Vieira. *Um estudo sobre ligaes do tipo YT de barras afastadas de sees tubulares circulares laminadas de aço*. PhD thesis, Estruturas, Universidade Estadual de Campinas, Campinas, 2007.

[9] R. F. Vieira, J. A. V. Requena, A. M. S. Freitas, and V. F. Arcaro. Numerical and experimental analysis of yield loads in welded gap hollow YT-joint. *Latin American Journal of Solids and Structures*, 6(4):363–383, 2009.

[10] J. Wardenier, Y. Kurobane, J. A. Packer, D. Dutta, and N. Yeomans. *Design guide for circular hollow section (CHS) joints under predominantly static loading – CIDECT*. Verlag TÜV Rheinland Gmbtt, 1991.